CME LIVE OPEN ACCESS

Journal of
Theoretical Physics & Mathematics Research

Research Article ISSN: 3065-8802

A Lattice Boltzmann Approach for Thermal Microflows

Anas Selmi[1,2*], Fedor Bukrev[2], Cristian Nagel[1] and Mathias J Krause[2]

[1]*Robert Bosch GmbH.*

[2]*Lattice Boltzmann Research Group, Karlsruhe Institute of Technology, Karlsruhe, Germany.*

Corresponding Author: Anas Selmi, Robert Bosch GmbH. Lattice Boltzmann Research Group, Karlsruhe Institute of Technology, Karlsruhe, Germany.

Received: 2026 Feb 26 **Accepted:** 2026 Mar 18 **Published:** 2026 Mar 30

Abstract

Microflows are of interest due to the increase in its applications in small devices. The effects of higher Knudsen numbers are studied on rarefied flows in an isothermal case then a thermal case in three dimensions. Boundary conditions are coupled to get a model that describes the slip at higher Knudsen numbers (higher than 0.01) and to improve its convergence with respect to mesh refinements. Various ways to calculate the slip effect are introduced and compared. Lastly, a simple thermal flow is simulated with the same previous approach and verified with a modified analytical solution to prove the benefits of the proposed boundary.

Keywords: Lattice Boltzmann Method, Rarefied Gas Flow, Higher Knudsen Number, Poiseuille Flow, Slip Boundary Condition, Thermal Creep

1. Introduction

Microflows have seen an increase in applications with the tendency to reduce the size of various components especially with the micro-electromechanical systems (MEMS). These systems usually contain gas at low pressure inside, which can have a significant influence on its overall behavior depending on how it affects the damping of moving structures or introduces stresses due to unwanted flows from various physical effects that become more important in such small scales. Moreover, it may not always be possible to simplify these structures to two dimensional models because of the various geometry properties that require all 3 dimensions to be modeled. The Knudsen number $K_n = \lambda/H$ can be used as a dimensionless number to describe the regime of the flow with the characteristic length in the geometry H and the mean free path $\lambda = (\mu/p)\sqrt{\pi RT/2}$, where μ is the viscosity, p the pressure, T the temperature and R the specific gas constant. For Kn<0.01 the flow can be considered as a continuum. For 0.01<Kn<0.1 the flow is classified as a slip flow, for 0.1<Kn<10 it is called transition flow and for Kn>10 it can be considered as a free molecular flow [1]. Since the mean free path is proportional to pre sure, a lower pressure with smaller dimensions leads to a high Knudsen number. That is why MEMS devices usually have higher Knudsen numbers and require simulation models that take this into account for an accurate numerical simulation of the physical effects. However, to simulate such complex structures, it is advised to first study the models in a more controlled environment where they can be tested and verified, then transferred to the desired complex geometry. This is what this work focuses on: testing models for high Knudsen numbers in a simple setup. Once that is done, in a later work, the same models will be used on complex MEMS geometries. In this context, the lattice Boltzmann method (LBM) which has seen an increase in popularity lately was also studied in the limit of higher Knudsen numbers and different boundary conditions were proposed to improve the results of the LBM in the slip and transition flow regimes in the form of slip boundary conditions as given by [1]. Various extensions have been proposed in the form of first and second order (in Knudsen number) slip with different scaling for the terms of the slip that were proposed in different papers to improve the results [1]. Other forms of boundary conditions were also proposed in the form of combined bounce back (the continuum boundary for LBM) specular reflection (CBBSR) [2]. A combination of bounce back and diffuse reflection was also proposed to mimic the Boltzmann equation boundary [3]. However, most of the boundaries were only studied in the simple two-dimensional case and the influence of the third dimension on the convergence of the method and the boundary are not clear. The goal of this paper is to focus on the three-dimensional case and propose a general way to implement slip boundary conditions and thermal creep effect. In fact, different ways to consider slip were introduced in and other works, but this paper doesn't focus on introducing a new slip model, instead it focuses on combining the existing slip models with an accurate way to implement velocities on boundaries in LBM [1]. Thus, even though we mainly focus on one slip model, the steps done in this work can be reproduced on any more complex slip model to improve its spatial accuracy. We focus on the

implementation of the kinetic theory slip model and how to combine it with the interpolated bounce back boundary to improve the convergence (in space) for general boundaries in 3dimensional space, which is much less characterized and studied in literature [4]. This method can be paired with any form of the slip models that compute the velocity on the boundary. Moreover, we test this implementation also with a different case, the thermal creep case, which is also of interest for higher Knudsen numbers. We derive an analytical solution for the pressure drop due to the creep effect and show its agreement with the simulation. The implementation is explained in detail throughout the work and simple steps are given in the form of algorithms to make it clear. The proposed method of combining interpolated bounce back boundary with slip boundary condition or thermal creep can work with any slip model that computes the velocity on the wall. For this purpose, we shortly introduce the lattice Boltzmann method, then we introduce the different boundary conditions needed, and we explain how they can be combined. Then we test the proposed boundaries for simple Poiseuille flow with a known analytical solution in the isothermal case. In the thermal case we extend the two-dimensional analytical solution to the three-dimensional case, and we compare it to simulation results. All the simulation and results in this work were done using the open-source code Open LB [5].

2. Theory

2.1. Lattice Boltzmann Method

The Boltzmann equation is an equation that characterizes the statistical behavior of a fluid by a probability distribution function (PDF) $f(\boldsymbol{x},\boldsymbol{v},t)$ that describes the density of particles at position $x \in \mathbb{R}^3$ and time t with velocity $v \in \mathbb{R}^3$. This distribution function, also called population, follows the equation [1]:

$$\frac{\partial f}{\partial t} + \boldsymbol{v} \cdot \frac{\partial f}{\partial \boldsymbol{x}} + \boldsymbol{F} \cdot \frac{\partial f}{\partial \boldsymbol{v}} = \Omega(f), \tag{1}$$

with collision operator $\Omega(f)$ and parameter space $(\boldsymbol{x},\boldsymbol{v},t)$. The complexity in solving the Boltzmann equation comes from two different sources: first the seven-dimensional parameter space $(\boldsymbol{x},\boldsymbol{v},t)$ and second the evaluation of the collision operator $\Omega(f)$.

The lattice Boltzmann method (LBM) can thus be seen as a discretized version of the Boltzmann equation, in that it discretizes the velocity space to a finite dimensional space. This means instead of the velocity being general $v \in \mathbb{R}^3$, only a finite set of velocities $\boldsymbol{v} \in \{\boldsymbol{c}_0,\ldots, \boldsymbol{c}_{q-1}\}$ is considered. This reduces the distribution function $f(\boldsymbol{x},\boldsymbol{v},t)$ to a set of q populations $f_i(\boldsymbol{x},\boldsymbol{v},t)$ for i=0,..., q - 1 which represent the density of particles with velocity $\boldsymbol{c}_i$ at position $\boldsymbol{x}$ and time t. Further discretizing in space and time (while ignoring external forces $\boldsymbol{F}$) gives the lattice Boltzmann equation (LBE) [6]:

$$f_i(\boldsymbol{x} + \boldsymbol{c}_i \Delta t, t + \Delta t) = f_i(\boldsymbol{x}, t) + \Omega_i(\boldsymbol{x}, t). \tag{2}$$

After solving this equation, it is possible to recuperate the macroscopic fluid density and velocity as the moments of the distribution function:

$$\rho(\boldsymbol{x}, t) = \sum_i f_i(\boldsymbol{x}, t), \tag{3}$$

$$\rho\boldsymbol{u}(\boldsymbol{x}, t) = \sum_i \boldsymbol{c}_i f_i(\boldsymbol{x}, t). \tag{4}$$

The collision operator can be chosen as the Bhantnagar-Gross-Krook (BGK) collision operator [6]:

$$\Omega_i(x, t) = -\frac{f_i(\boldsymbol{x}, t) - f_i^{eq}(\boldsymbol{x}, t)}{\tau} \Delta t, \tag{5}$$

with relaxation time τ. The equilibrium distribution function f_i^{eq} is given by:

$$f_i^{eq}(\boldsymbol{x}, t) = w_i \rho \left(1 + \frac{\boldsymbol{u} \cdot \boldsymbol{c}_i}{c_s^2} + \frac{(\boldsymbol{u} \cdot \boldsymbol{c}_i)^2}{2c_s^4} - \frac{\boldsymbol{u} \cdot \boldsymbol{u}}{2c_s^2}\right), \tag{6}$$

where w_i are the Hermite quadrature weights associated to the lattice velocities $\boldsymbol{c}_i$ and $\boldsymbol{c}_s$ is the speed of sound corresponding to the velocity set. The velocity sets are denoted by DdQq where d is the dimension and q is the number of discrete velocities. For the most common velocity sets e.g. D2Q9 or D3Q19 the speed of sound squared c_s^2 is:

$$c_s^2 = \frac{1}{3}\left(\frac{\Delta x}{\Delta t}\right)^2, \tag{7}$$

and the speed of sound links the relaxation time to the kinematic viscosity of the fluid by $\nu = c_s^2\left(\tau - \frac{\Delta t}{2}\right)$.

To solve the LBM in a practical way, equation (2) can be divided into a collision and streaming steps to give the simple algorithm [6]:

1. Compute macroscopic variables $\rho(\boldsymbol{x},t)$ and $\boldsymbol{u}(\boldsymbol{x},t)$.
2. Calculate the new equilibrium distribution function f_i^{eq}.
3. Perform the collision step:

$$f_i^c(\boldsymbol{x}, t) = f_i(\boldsymbol{x}, t) + \Omega_i(\boldsymbol{x}, t). \tag{8}$$

4. Perform the streaming step:

$$f_i(\boldsymbol{x} + \boldsymbol{c}_i \Delta t, t + \Delta t) = f_i^c(\boldsymbol{x}, t). \tag{9}$$

5. Apply boundary conditions.
6. Increment time step to t+Δt and go back to step 1.

Now the only missing block in solving the LBM is to define the boundary conditions and how they are implemented.

2.2. Boundary Conditions

There are different ways to define boundary conditions for the LBM in the continuum limit. They are usually called bounce back boundary conditions or no-slip boundary conditions. They usually consist of setting the velocity on the wall to 0 (for a non-moving wall, otherwise equal to the wall velocity in a more general case). In this work we focus

on the boundary condition introduced by since it offers second order convergence in space discretization [4]. This proves especially appealing for curved boundaries. On the other hand, the effect of high Knudsen numbers in the flow is generally introduced through boundary conditions, which also benefits from the accuracy order of the boundary. Thus the first step is to look at the boundary condition introduced by which we will call Bouzidi boundary condition from this point onward conforming to the naming also used in the source code used for simulations [4,5].

2.2.1. Bouzidi Boundary Condition

The Bouzidi boundary condition is a way to set the no slip condition on walls that improves on the general bounce-back boundary condition for general boundary profiles, which leads to a significant improvement in accuracy when the wall is curved. That is why we focus on this boundary condition is this work and try to extend it to take into account slip effects that appear at higher Knudsen numbers.

To introduce this boundary condition, we define a variable $q_B = |\overline{xx_b}|/|\overline{xx_s}|$ (see Figure 1) which describes the fraction of the cell inside the fluid in each lattice direction. In this case, $\boldsymbol{x}$ describes the cell at which the boundary value is to be calculated, $\boldsymbol{x}_b$ is the point located on the wall in the direction of the current lattice velocity and $\boldsymbol{x}_s$ is the cell inside the solid in the same direction as $\boldsymbol{x}_b$.

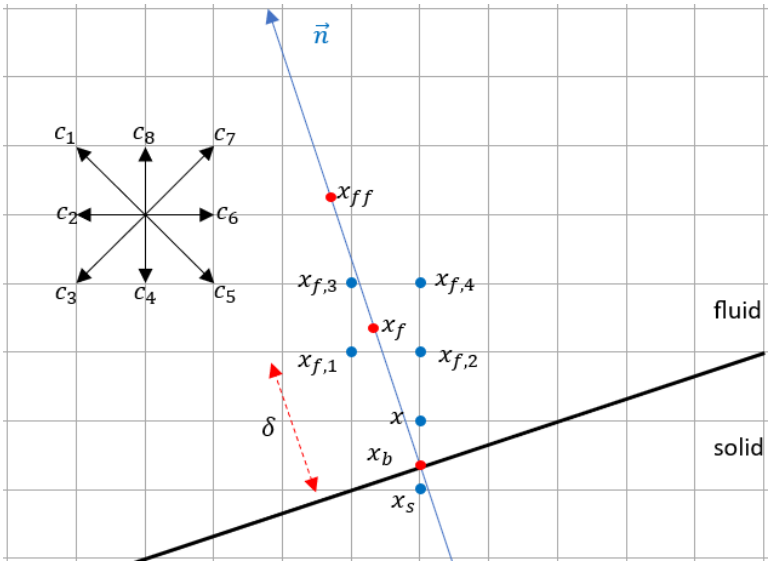

Figure 1: Lattice representation for the wall at x for lattice velocity c_4. The points marked on the grid represent cells in the discretized domain. δ is the distance in the normal direction between the boundary node and the first fluid node, and $x_{f,i}$ are the cells surrounding x_f since the latter isn't guaranteed to land exactly on a cell

The value of $q_B = \frac{|xx_b|}{|xx_s|}$ can range from 0 to 1, and it is defined for each lattice direction (see Figure 1 for the lattice velocity $\boldsymbol{c}_4$). For the directions that have no wall, this can be defined as -1. To set the bounce back boundary condition, we define:

$$f_{i'}(\boldsymbol{x}, t+\Delta t) = \begin{cases} 2q_B f_i^c(\boldsymbol{x},t) + (1-2q_B) f_i^c(\boldsymbol{x}-\boldsymbol{c}_i\Delta t, t), & q_B < \frac{1}{2} \\ \frac{1}{2q_B} f_i^c(\boldsymbol{x},t) + \frac{2q_B-1}{2q_B} f_{i'}^c(\boldsymbol{x},t), & q_B \geq \frac{1}{2} \end{cases} \quad (10)$$

with x the fluid node adjacent to the wall where the boundary value is calculated, i' the index of the reversed direction to i such that $\boldsymbol{c}_{i'} = -\boldsymbol{c}_i$, $\boldsymbol{x} + \boldsymbol{c}_i \Delta t$ being a solid node ($\boldsymbol{x}_s$ in Figure 1) and $f_i^c(\boldsymbol{x},t)$ the populations after collision and before propagation as shown in equation (8). Since q_B is defined for every cell near the boundary separately, this allows for general curved boundaries, and in the special case that $q_B = 1/2$ everywhere, equation (10) falls back to the usual halfway bounce back known for LBM.

2.2.2. Bouzidi Velocity Boundary Condition

The next type of boundary also introduced in [4] is a simple modification of the boundary defined in (10) to define a fluid velocity on the wall by a given value instead of 0. This is especially useful in the continuum regime for moving walls but is also interesting in slip or transition regimes since it can be used to write velocity slip on walls.

If we consider the velocity $\boldsymbol{u}_0$ of the fluid on the wall (on node x in Figure 1), the distribution function on this node can be updated by equation (10) to which we add the following terms:

$$\begin{cases} 2\alpha_i \boldsymbol{c}_i \cdot \boldsymbol{u}_0, & q_B < \frac{1}{2} \\ \frac{1}{q_B}\alpha_i \boldsymbol{c}_i \cdot \boldsymbol{u}_0, & q_B \geq \frac{1}{2} \end{cases} \quad (11)$$

with $\alpha_i = w_i / c_s^2$ coefficients depending on the discrete lattice velocity set.

2.2.3. Slip Boundary Condition

Our newly proposed boundary condition extends off the

Bouzidi boundary in equations (10) and (11) to account for slip effects. It is composed of two main components, the first is the Bouzidi boundary which describes how to define a velocity near a wall for general wall profiles, and the second being how to compute the slip value.

In fact, for flows in the continuum regime (Kn<0.01) the no-slip boundary is a good approximation for the fluid-solid interface. However, as the Knudsen number increases, experiments and simulation of the linearized Boltzmann equation have shown that there starts to appear a relative velocity between the wall and fluid [7]. To capture this effect, we use the velocity slip boundary [1]:

$$\boldsymbol{u}_{slip} = \boldsymbol{u}_b = \lambda_{eff} \frac{\partial \boldsymbol{u}}{\partial \boldsymbol{n}}, \tag{12}$$

with the effective mean free path $\lambda_{eff} = \left(\frac{1}{\lambda} + \frac{c}{H}\right)^{-1}$ defined as in [8] with constant $c \in [0,1]$ and $\boldsymbol{n}$ the inner normal vector to the boundary. In the case of $\boldsymbol{c} = 0$ the boundary is called Maxwell's first order slip boundary condition.

To implement this boundary in a simulation, namely the LBM introduced in the previous section, we need a way to compute the partial derivative $\frac{\partial \boldsymbol{u}}{\partial \boldsymbol{n}}$, for this we propose 3 different variants:

• Bouzidi slip zeroth degree (BS0):

The simplest way to implement the slip velocity is to consider it as a fraction of the neighbor velocity $\boldsymbol{u}_f$ with a constant $c_{st} \in [0,1]$ (see Figure 1):

$$\boldsymbol{u}_{slip} = c_{st}\, \boldsymbol{u}_f. \tag{13}$$

This doesn't really approximate the gradient in equation (12), but it is a way t introduce slip with a free to choose parameter that is similar to the combined bounce back specular reflection introduced in other works that focus on slip in LBM, that is why it is called zeroth degree [2]. For const=0 this will come back to the no slip boundary and for const=1 this will give a full slip, i.e. the absence of shear forces on the wall.

• Bouzidi slip first degree (BS1):

To get a first degree (in space) approximation of the gradient $\partial \boldsymbol{u}/\partial \boldsymbol{n}$, we consider the forward difference rule (see Figure 1 for indices):

$$\frac{\partial \boldsymbol{u}}{\partial n} = \frac{\boldsymbol{u}_f - \boldsymbol{u}_b}{\delta}. \tag{14}$$

This gives the value of the velocity on the boundary:

$$\boldsymbol{u}_{slip} = \lambda_{eff} \frac{\boldsymbol{u}_f - \boldsymbol{u}_b}{\delta}, \tag{15}$$

which can be transformed to:

$$\boldsymbol{u}_{slip} = \frac{\lambda_{eff}}{\lambda_{eff} + \delta} \boldsymbol{u}_f. \tag{16}$$

• Bouzidi slip second degree (BS2):

For the second-degree space discretization of the gradient, we need 2 neighbors instead of only one:

$$\frac{\partial \boldsymbol{u}}{\partial \boldsymbol{n}} = \lambda_{eff} \frac{1}{\delta} \left(-\frac{3}{2} \boldsymbol{u}_b + 2\boldsymbol{u}_f - \frac{1}{2} \boldsymbol{u}_{ff} \right). \tag{17}$$

We can now replace this in equation (12) and after grouping $\boldsymbol{u}_s$ on the left-hand side, we get:

$$\boldsymbol{u}_{slip} = \frac{\lambda_{eff}}{\delta + \frac{3}{2}\lambda_{eff}} \left(2\boldsymbol{u}_f - \frac{1}{2} \boldsymbol{u}_{ff} \right). \tag{18}$$

Note that the neighbors in normal direction $\boldsymbol{u}_f$ and $\boldsymbol{u}_{ff}$ don't necessarily fall on grid nodes, that is why an interpolation is necessary to get the values along the normal, additionally $\delta = 2\Delta x$ is chosen such that the second neighbor doesn't fall in the same neighborhood as the first one. In fact, in 2D it is possible to choose a smaller step $\delta = 1.5\Delta x$ since the maximum distance in a 2D square with side 1 is $\sqrt{2}$, but in 3D this works best.

After introducing the gradient computation methods, we now combine the slip boundary condition with the Bouzidi velocity boundary from equation (11) to get a good approximation on general boundaries. We summarize the algorithm in the following steps:

For each lattice velocity $\boldsymbol{c}_i$:

1. Check if there exists a physical boundary with $0 \le q_B < 1$. If yes, go to next step, otherwise go to next lattice velocity.
2. Find the normal vector on the boundary pointing inside the fluid $\boldsymbol{n}$.
3. Step a distance δ in the normal vector direction and interpolate the neighbors to find the velocity at $\boldsymbol{x}_b + \delta \cdot \boldsymbol{n}$. In 2D that would be 4 neighbors, and in 3D 8 neighbors:

$$\boldsymbol{u}_f = \sum_j V_j \boldsymbol{u}_{f,j}, \tag{19}$$

with $\boldsymbol{u}_f$ the velocity at point $\boldsymbol{x}_f$ and $\boldsymbol{u}_{fj}$ the velocities on the nodes around $\boldsymbol{x}_f$, the weights for the neighbors are computed by:

$$V_j = \left(\Delta x - |x_f - x_{f,j}|_x\right)\left(\Delta x - |x_f - x_{f,j}|_y\right)\left(\Delta x - |x_f - x_{f,j}|_z\right), \tag{20}$$

with $|\cdot|_x$, $|\cdot|_y$ and $|\cdot|_z$ denoting the x, y and z coordinates of the vector inside.

4. If necessary, compute the velocity $\boldsymbol{u}_{ff}$ at the second neighbor along the normal at $\boldsymbol{x}_b + 2\delta \cdot n$.
5. Compute the value of the velocity at the boundary $\boldsymbol{u}_b = \boldsymbol{u}_{slip}$ for the current lattice direction $\boldsymbol{c}_i$ using one of the equations (13), (16) or (18).
6. To make sure there is no fluid crossing the boundary, project the calculated velocity on the tangent:

$$\boldsymbol{u}_{b,t} = \boldsymbol{u}_b - (\boldsymbol{u}_b \cdot \boldsymbol{n})\boldsymbol{n}, \tag{21}$$

7. Use this new velocity on the boundary $\boldsymbol{u}_{b,t}$ for the Bouzidi

velocity boundary as in equation (11) combined with (10) in place of $\boldsymbol{u}_0$ to write it for the current lattice velocity $\boldsymbol{c}_i$.
8. Increment i to go to the next lattice velocity $\boldsymbol{c}_{i+1}$ and go back to step 1.

The representation in Figure 1 shows the various variables for the lattice direction $\boldsymbol{c}_4$, and in the case drawn there, this needs to be repeated for $\boldsymbol{c}_5$ too.

2.3. Thermal Flow Simulation Using LBM

The LBM as was introduced until now can only simulate isothermal flows. However, in fluid simulation, many use cases require solving both flow and temperature equations for an accurate estimate of the reality. This can be done using the LBM by introducing another equation for the advection diffusion problem and introducing a coupling scheme to account for the influence of the flow on the temperature and the other way around [6,9,10].

This is called the double distribution method since it consists of defining a second distribution function g_i, with i =1,⋯, q whose 0th moment represents the temperature:

$$T(x,t) = \sum_i g_i, \tag{22}$$

and that obeys the LB equation:

$$g_i(x + c_i\Delta t, t + \Delta t) - g_i(x,t) = \Omega_i(x,t) + Q_i(x,t), \tag{23}$$

where $Q_i(x,t)$ is a source term and Ω_i is the collision operator which can also be chosen as the BGK operator

$$\Omega_i(x,t) = -\frac{g_i(x,t) - g_i^{eq}(x,t)}{\tau_g}, \tag{24}$$

with the equilibrium distribution function:

$$g_i^{eq} = w_i T\left(1 + \frac{\boldsymbol{c_i}\cdot\boldsymbol{u}}{c_s^2}\right). \tag{25}$$

Furthermore, similar to the first LBE used for solving the flow velocity, the relaxation time in the thermal LBE can be linked to the thermal diffusivity of the fluid by $D = c_s^2\left(\tau_g - \frac{\Delta t}{2}\right)$.

Note that the set of discrete velocities for solving this equation doesn't need to be the same as the velocity set for solving the LBE for fluid flow from the previous section. In fact, often a smaller set is chosen for the temperature equation (such as D2Q5 or D3Q7) [6].

For the coupling between equations (2) and (23), one way is already available with the model in equation (25), and that is the influence of the fluid velocity on the spread of the temperature, or also called advection. The other direction, i.e. the influence of the temperature on the fluid, needs to be implemented. This is usually done by the Boussinesq approximation [6], which assumes small temperature and density changes:

$$\rho(T) \approx \rho_0\big(1 - \alpha(T - T_0)\big). \tag{26}$$

The influence of the change in density can then be added as an external force in the fluid LBE, also called Buoyancy force:

$$\boldsymbol{F}_b = (\rho(T) - \rho_0)\boldsymbol{g}, \tag{27}$$

with g the earth gravitational field.

This approximation however becomes less reliable the higher the Knudsen number gets, as the influence of gravity on the fluid becomes negligeable. This has been investigated and shown in on a Micro-electromechanical sensor (MEMS), specifically an accelerometer [11]. That is why, for an increase in Knudsen number in slip or transion regime another way of coupling is introduced, called the thermal creep [1]. This effect describes that fluid particles on a wall with a temperature gradient have different momentum dependent on the temperature, which creates a creep of the fluid from the cold to hot regions on the wall [12].

A simple way to explain this effect (as shown in [1]) is by looking at t he temperature as a multiple of the square average molecular speed $T \propto \bar{\boldsymbol{c}}^2$. The mass fluxes at the hot and cold sides are then

$$mn_1\bar{\boldsymbol{c}}_1 \text{ and } mn_2\bar{\boldsymbol{c}}_2, \tag{28}$$

where m is the mass of the gas particles and n the number density (number of molecules per unit volume) with $n \propto \rho$. Then

$$\frac{mn_1\bar{\boldsymbol{c}}_1}{mn_2\bar{\boldsymbol{c}}_2} \approx \frac{\rho_1}{\rho_2}\left(\frac{T_1}{T_2}\right)^{0.5} = \frac{P_1}{P_2}\left(\frac{T_2}{T_1}\right)^{0.5} \leq 1, \tag{29}$$

with $P = \rho RT$ and $\frac{P_1}{P_2} = 1$.

This effect can be macroscopically described as an increase in the velocity on the walls given by:

$$\boldsymbol{u}_c = \frac{3}{4}\frac{\mu R}{p}\frac{\partial T}{\partial \boldsymbol{s}}, \tag{30}$$

where $\boldsymbol{u}_c$ is the tangential creep velocity and $\partial T / \partial s$ is the temperature gradient along the boundary. This can be added with the slip boundary condition introduced in the previous section in equation (12) to form a boundary condition for thermal flows with higher Knudsen numbers. Additionally, equation (30) contains a gradient of the temperature of the fluid on the wall, which can be used as a way to include the influence of the temperature on the fluid for the coupling. The velocity calculated from equation (35) can also be applied in the same way the slip velocity is applied, namely using the same procedure as in section 2.2.3 while replacing the normal vector $\boldsymbol{n}$ by the tangential $\boldsymbol{s}$. In this context, there is a problem that needs to be solved. In fact, the inner normal vector to a boundary in 3D is unique, but the wall has an infinite number of tangential vectors.

To solve this problem, we simply choose the vector

$$\boldsymbol{s}_x = (1,0,0)^T, \tag{31}$$

parallel to the x-axis. Then we compute the tangent to the boundary $\mathbf{s}_1$ as

$$\boldsymbol{s}_1 = \boldsymbol{s}_x - (\boldsymbol{s}_x \cdot \boldsymbol{n})\boldsymbol{n}, \tag{32}$$

which is the projection of the unit vector $\boldsymbol{s}_x$ on the boundary tangent. $\boldsymbol{s}_1$ is thus orthogonal to n and it is possible to compute the thermal creep from equation (28) along it. Additionally, we compute a second tangent vector $\boldsymbol{s}_2$ as

$$\mathbf{s}_2 = \mathbf{s}_1 \times \boldsymbol{n}, \tag{33}$$

then compute the thermal creep along it too. And then we add both components each multiplied by its vector

$$\boldsymbol{u}_c = \frac{3}{4}\frac{\mu R}{p}\left[\frac{\partial T}{\partial \boldsymbol{s}_1}\boldsymbol{s}_1 + \frac{\partial T}{\partial \boldsymbol{s}_2}\boldsymbol{s}_2\right]. \tag{34}$$

In case $\boldsymbol{s}_x$ is parallel to n choose another vector, e.g. $\boldsymbol{s}_x$ = (1,-1,0)^T.

This choice of tangent vectors prioritises the tangent parallel to the coordinate system. This choice makes sense because the velocity set of the temperature LBE is usually D3Q7 in 3D. This means that the temperature spreads in the 6 directions parallel to the axes, but not in the diagonal direction. So computing the temperature gradient along these directions is the most effective.

3. Numerical Results: Cylinder Poiseuille Flow in 3D

To verify the results from the previous section, we simulate a 3D Poiseuille flow in a cylinder pipe as shown in Figure 2 using the LBM software Open LB [5]. The center of the first face (inlet) of the cylinder lies in (0,*R*,*R*) and the center of the second face (outlet) lies in (*L*,*R*,*R*) in the coordinate system (*x*,*y*,*z*) as shown in the figure. A transformation can be performed to get the cylinder coordinates (x,r,φ) ∈ [0,*L*] × [0, *R*] × [0,2π) with $r^2 = (y - R)^2 + (z - R)^2$ and $\varphi = tan^{-1}\left(\frac{y-R}{z-R}\right)$. The geometry as well as physical parameters are given in Table 1.

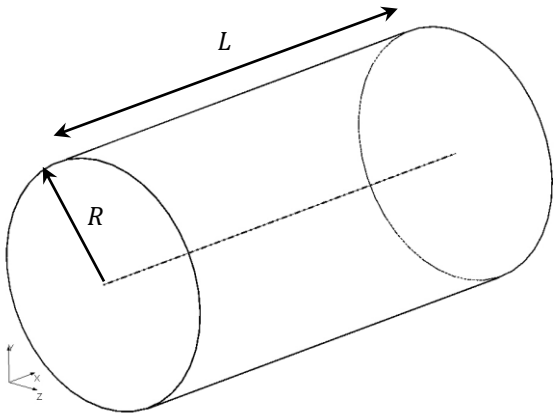

Figure 2: Simulation Geometry

Parameter	Symbol	Value
Radius	R	0.5m
Length	L	2m
Density	ρ	1 kg/m^3
Max velocity	U_{max}	1 m/s
Kinematic viscosity	ν	0.1 m^2/s
Dynamic viscosity	$\mu = \rho\nu$	0.1 Pa.s
Relaxation time	τ	0.8

Table 1: Simulation Parameters

The analytical solution of the flow with no-slip boundary as it is already implemented in [5] is:

$$u(r) = U_{max}\left(1 - \frac{r^2}{R^2}\right), \tag{35}$$

with

$$U_{max} = \frac{GR^2}{4\mu} = -\frac{\Delta p}{L}\frac{R^2}{4\mu}, \tag{36}$$

where $G = -\Delta p / L$ is the pressure force.

To verify the accuracy of the boundary condition, we first need to modify the analytical solution to account for the slip

effects. This is done by considering the new solution for slip flows in [1] up to first order in Kn, which after some slight variable changes looks:

$$u(r) = U_{max}\left(1 - \frac{r^2}{R^2} + 4Kn\right). \quad (37)$$

It is important to note that normally, changing the Knudsen number has an influence of the other physical parameters such as density since the mean free path $\lambda = \frac{\rho}{p}\sqrt{\frac{\pi}{2RT}}$ depends on other parameters in its macroscopic definition [8]. However, in this work we only consider the influence of the Knudsen number on the wall velocity, i.e. the Knudsen number only has an effect on the slip boundary we introduced and not the bulk of the fluid. This helps simplify the simulation and the evaluation of the convergence. Additionally, to better characterize the convergence order and accuracy of the boundary, we consider two ways to generate a flow inside the pipe shown in Figure 2: forced flow, and non-forced flow. Both these flow types can be simulated in Open LB with the same code, simply by adding an external force in the first case. The goal of testing both flow cases it to minimize the effect of inlet and outlet boundary conditions in the case of forced flow, since in this case we only define periodic boundaries on the left and right which reduces the complexity of the problem and the possible error sources at the corner cells where different boundaries meet.

3.1. Forced Flow

In this section, the flow is generated by a constant pressure force applied on the fluid as defined in equation (36). This case is of interest to study since from a simulation point of view it is one of simplest options. In fact, the only boundary that needs to be defined is the outer wall at $(x, r = R, \varphi)$ with $x \in [0, L]$ and $\varphi \in [0, 2\pi)$. The inlet at $x = 0$ and outlet at $x = L$ can be set to be periodical, i.e. what exits the domain comes back in. This reduces the complexity of additional boundaries and only requires the use of external force in LBM. The flow solution writes:

$$u(r) = \frac{GR^2}{4\mu}\left(1 - \frac{r^2}{R^2} + 4Kn\right), \quad (38)$$

with $U_{max} = GR^2 / 4\mu$.

Note that with increasing Knudsen number, the maximum velocity at $r = 0$ also increases. To avoid this and get a constant maximum velocity of $U_{max} = 1\ m/s$ for all Knudsen numbers (as was chosen in Table 1) we need to modify the pressure force G for every Knudsen number to account for the increase in velocity due to slip. This can be done by considering the velocity in the center axis of the pipe:

$$u(r = 0) = \frac{GR^2}{4\mu}(1 + 4Kn) = U_{max,Kn}. \quad (39)$$

To avoid confusion, we denote $U_{max,Kn}$ the actual maximum velocity at the center axis of the pipe at any given Kn, which is kept constant to 1 m/s. Modifying the previous equation gives the corresponding pressure force:

$$G = \frac{4\mu U_{max,Kn}}{R^2(1 + 4Kn)}. \quad (40)$$

With this new pressure force, and the analytical solution (38), we always get $U_{max.Kn}$ as maximum velocity, and the only value that changes is the velocity on the wall:

$$u(r = R) = \frac{GR^2}{4\mu}4Kn = \frac{4Kn}{1 + 4Kn}. \quad (41)$$

Choosing the same parameters as in Table 1 with $U_{max,Kn} = 1m/s$ instead of U_{max}, we get the following values for different Knudsen numbers:

Knudsen number	Velocity on wall (m/s)	Force (N)
0	0	1.6
0.05	0.1667	1.333
0.25	0.5	0.8

Table 2: Influence of Knudsen number on wall Velocity and Pressure Force

Next, to verify our boundary condition, we perform an experimental order of convergence (EOC) analysis of the simulation with the different discrete gradient forms. We take as benchmark the Bouzidi velocity boundary (11) as we can give it the analytical velocity on wall for the simulation. Then we calculate L1, L2 and Linf error norms as follows (replacing L_p with the corresponding norm) with $\boldsymbol{u}_{sol}$ from equation (38) and $\boldsymbol{u}_{sim}$ taken at $L/2$:

$$\mathrm{E}_{L_p} = \|\boldsymbol{u}_{sim} - \boldsymbol{u}_{sol}\|_{L_p}. \quad (42)$$

The first benchmark is at $Kn = 0$. Note that $Kn = 0$ is just a notation used for continuum flows and that it means $Kn \to 0$ rather than exactly 0 since λ can't be less than the particle diameters. The EOC for this value of Kn is done as a benchmark and check for the code structure to make sure it works at continuum limit and it falls back to the no-slip Bouzidi boundary (see Figure 3). It is important to note here that for all our simulations, we use the diffusive scaling in all our simulations $\Delta t \propto \Delta x^2$, this means doubling the resolution results in 4 times smaller time step. This guarantees that the LBM is second order accurate in space in the bulk of the flow [6].

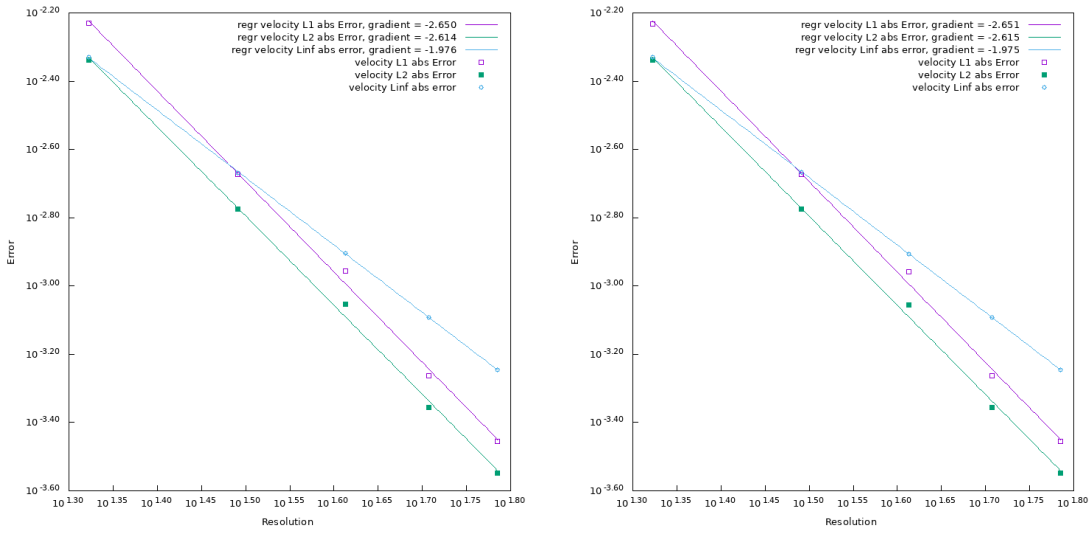

(a) (b)

Figure 3: EOC at *Kn* = 0 for forced flow. (a) Bouzidi velocity, (b) Bouzidi slip

Next, we look at a higher Knudsen number Kn=0.05. The EOC plots are shown in Figure 4. The Bouzidi slip 0th degree from equation (13) and shown in (b) does not converge well with increasing resolution. This is to be expected, as although it is similar to the Bouzidi slip 1st degree from equation (16), the constant with which the neighbor velocity is multiplied is not the same. In fact, in the 0th degree, the constant is chosen (0.5 in the figure), and it stays constant over all resolutions. However, in the 1st degree variant, the constant is $\frac{\lambda_{eff}}{\lambda_{eff}+\delta}$ which has a resolution dependency hidden in $\delta = 2\Delta x$, that is the main difference between these two boundaries. Note that with 1st degree gradient we get a convergence of first order, and with the 2nd degree gradient we get a much better convergence order (close to second degree).

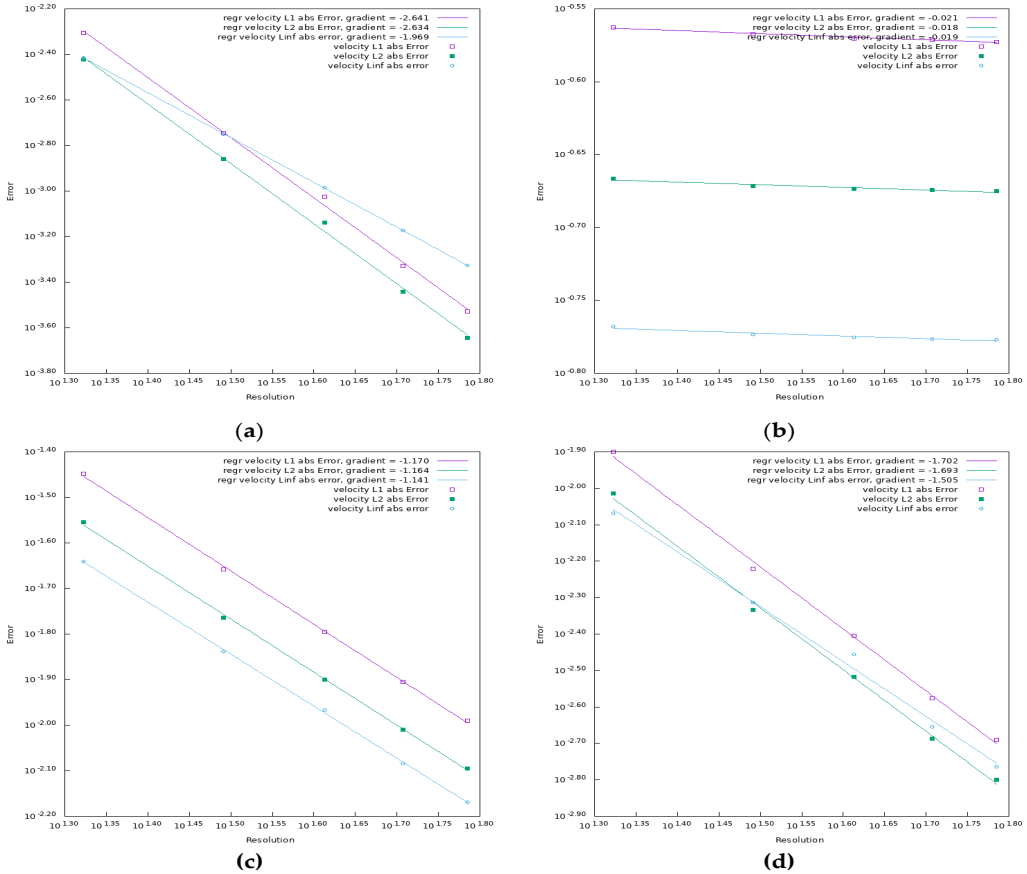

(a) (b)

(c) (d)

Figure 4: EOC for forced flow at Kn=0.05: (a) Bouzidi velocity with analytical solution on boundary; (b) Bouzidi slip 0th degree with c=0.5; (c) Bouzidi Slip 1st degree (c=0); (d) Bouzidi slip 2nd degree

We can also look at the velocity profile at $L/2$ and compare it to the analytical solution. This can be seen in Figure 5. The Bouzidi slip with 2nd degree gradient gives the best results. The jump at y = 0 and y = R is due to the nature of the boundary condition and is even visible when using the analytical solution of the slip on the wall. However, the higher the resolution, the less visible is this jump.

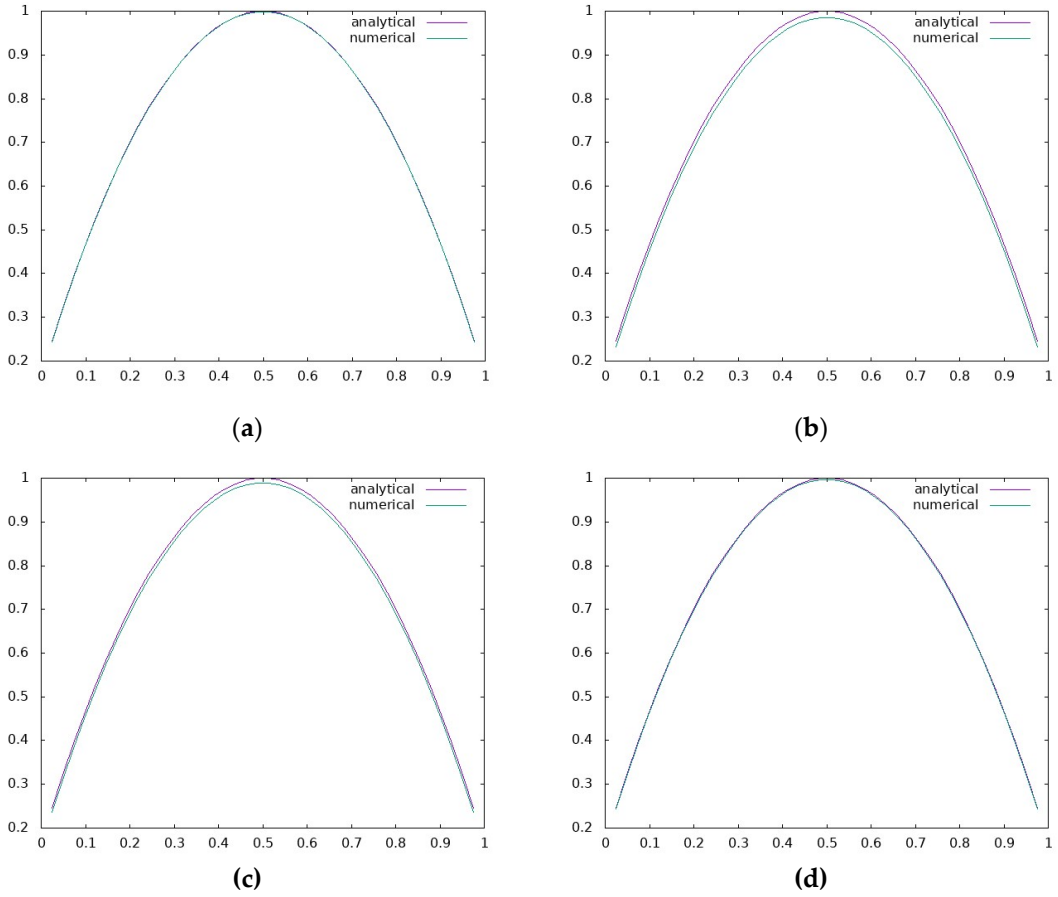

Figure 5: Velocity profile along y-axis at z=R and *Kn*=0.05 for resolution of 41: (a) Bouzidi velocity with analytical solution on boundary; (b) Bouzidi slip 0th degree with c=0.5; (c) Bouzidi Slip 1st degree (c=0); (d) Bouzidi slip 2nd degree

Increasing the Knudsen number does seem to worsen the convergence order slightly, but it is still better than first order (see Figure 6). Additionally, the 0th degree slip was not plotted as it doesn't converge with resolution as shown in Figure 4.

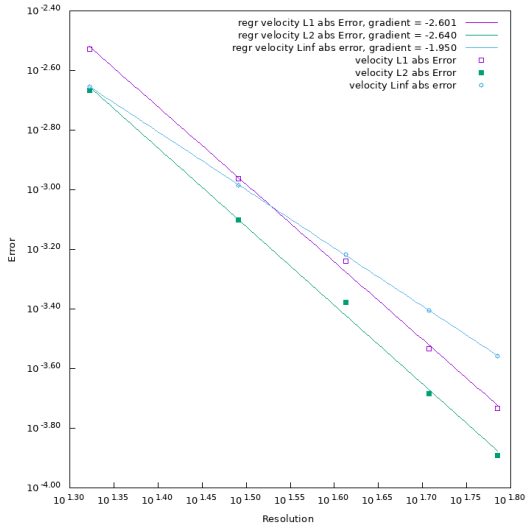

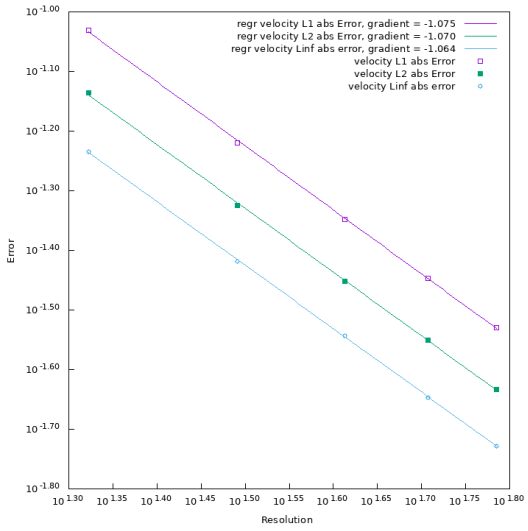

(b)

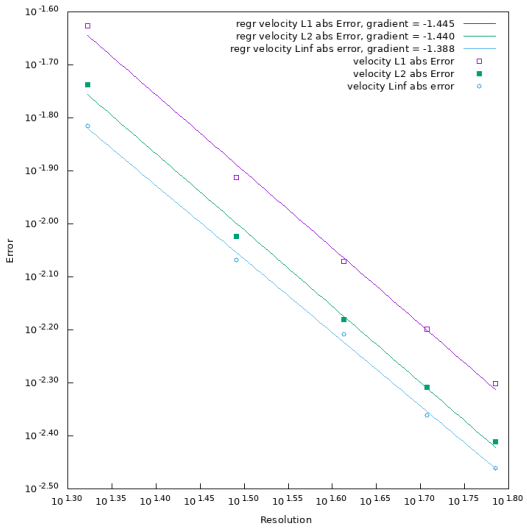

(c)

Figure 6: EOC for forced flow at *Kn*=0.25: (a) Bouzidi velocity with analytical solution on boundary; (b) Bouzidi Slip 1st degree (c=0); (c) Bouzidi slip 2nd degree

3.2. Non-Forced Flow

The non-forced case is similar to the forced case with $\Delta p = -GL$, but instead of the flow being caused by an external force, it is generated by an inlet velocity on the left ($x = 0$) and free outlet pressure on the right ($x = L$). The inlet boundary conidition is set to an interpolated velocity boundary (setInterpolated Velocity Boundary in open LB [5]) with the analytical velocity profile:

$$u(r) = \frac{U_{max,Kn}}{1+4Kn}\left(1 - \frac{r^2}{R^2} + 4Kn\right), \tag{43}$$

and free pressure outlet (setInterpolatedPressureBoundary in [5]) with a pressure difference of:

$$\Delta p = -\frac{4\mu L U_{max,Kn}}{R^2(1+4Kn)}. \tag{44}$$

For simplicity's sake, and since only the pressure difference is important, we choose the pressure at $x = 0$ to be:

$$p_0 = -\Delta p = -\frac{4\mu L U_{max,Kn}}{R^2(1+4Kn)}, \tag{45}$$

While the pressure at $x = L$ is set to $p_1 = p(x = L) = 0$. The solution for the pressure profile in this case is the linear function:

$$p(x) = -\frac{p_0}{L}x + p_0. \tag{46}$$

We get the following values for different Knudsen numbers:

Knudsen number	Velocity on wall (m/s)	Pressure p_0 in Pa
0	0	3.2
0.05	0.1667	2.667
0.15	0.375	2
0.25	0.5	1.6

Table 3: Velocity and Pressure Values for Given Knudsen Number

The EOC plots like in the previous section show convergence better than first order as is shown in Figure 7 and Figure 8.

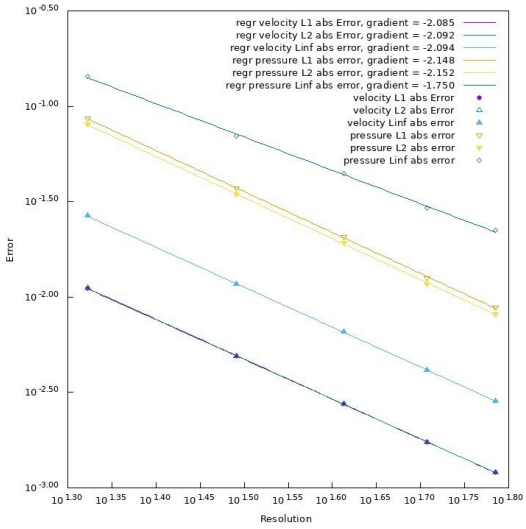

(a)

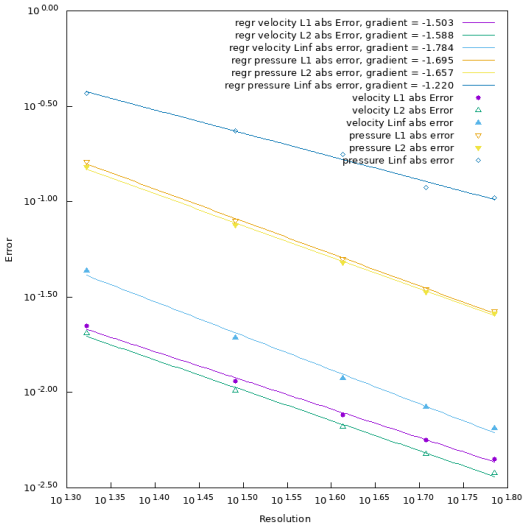

(b)

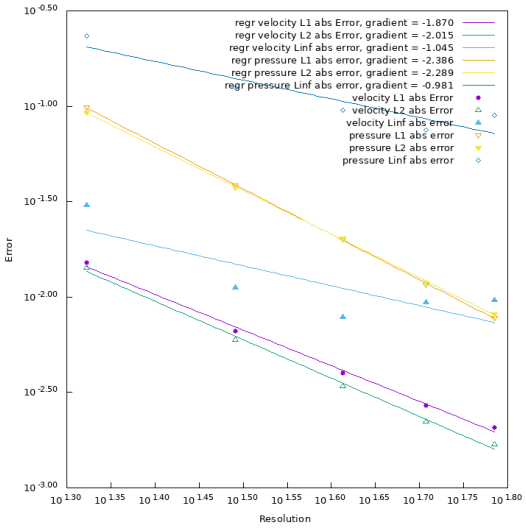

(c)

Figure 7: EOC for non-forced flow at Kn=0.05: (a) Bouzidi velocity with analytical solution on boundary; (b) Bouzidi slip 1st degree (c=0); (c) Bouzidi Slip 2nd degree

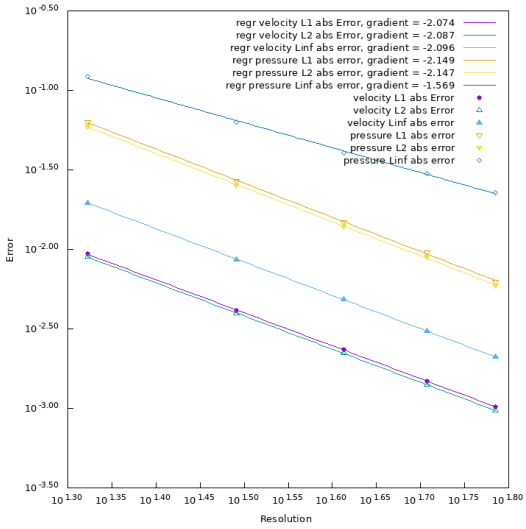

(a)

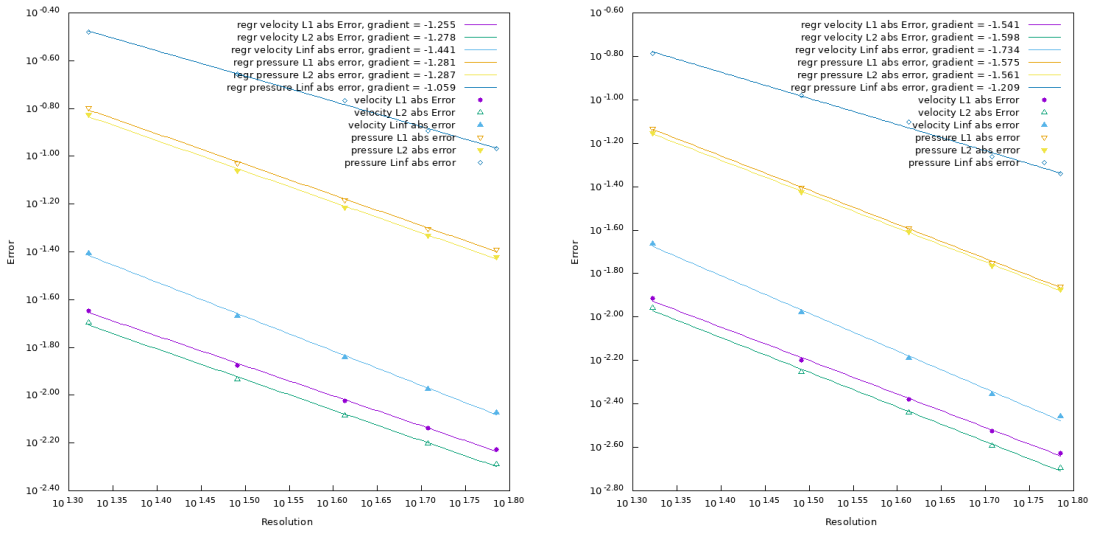

(b) (c)

Figure 8: EOC for non-forced flow at Kn=0.25: (a) Bouzidi velocity with analytical solution on boundary; (b) Bouzidi slip 1st degree (c=0); (c) Bouzidi Slip 2nd degree

3.3. Thermal Poiseuille flow

Parameter	Symbol	Value
Radius	R	0.5 µm
Length	L	2 µm
Mean free path	λ	0.053 µm
Relaxation time	τ	0.75
Specific gas constant	R_{spec}	287 J/(Kg.K)
Dynamic viscosity	μ	18.13 µPa.s
Thermal conductivity	κ	0.015 W(m.K)

Table 4: Thermal Poiseuille simulation parameters. Other Parameters not Listed in this Table Can be Cal-cuLated Using These Values

In this section we simulate a Poiseuille flow as shown in Figure 2 with a temperature gradient along the x-axis. Here, we close the inlet and outlet so that we get a closed domain, and we downscale the dimensions by 10^{-6} to obtain a Knudsen number of Kn=0.053 without the need for a near-vacuum pressure. In other words, the temperature at $x = 0$ is set to $T_1 = 293K$ and at $x = L$ to $T_2 = 293.5K$ respectively and the domain is set to be closed at $x = 0$ and $x =$ L. The walls along the x axis get a linear scaling temperature bounadry from T_1 to T_2. All temperature boundaries are applied in a Dirichlet-type boundary condition [5]. We simulate the flow that is generated by the temperature gradient using the parameters in Table 4, and we verify with the pressure difference created by the temperature gradient. The solution for the pressure difference was given in for a 2D flow, but since we simulate a 3D cylinder flow, we need to do some modifications [1]. The first difference to the 2D case is in the solution of the velocity profile for the isothermal case (see equation (37)). Additionally, to calculate the pressure difference, first we need to determine the mass flow rate which can be calculted in the cylinder coordinate system Figure 2 by:

$$\dot{M} = 2\pi\rho \int_0^R u(r) r dr, \tag{47}$$

with the velocity $u(r)$ given by equations (37) and (30) summed together:

$$u(r) = -\frac{\Delta p}{L}\frac{R^2}{4\mu}\left(1 - \frac{r^2}{R^2} + 4Kn\right) + \frac{3}{4}\frac{\mu R}{p}\frac{\partial T}{\partial x}. \tag{48}$$

This is in fact different to the 2D case where the mass flow rate is given by

$$\dot{M} = \rho \int_0^h u(y) dy. \tag{49}$$

Recalculating the mass flow rate by replacing equation (48) in (47), we get

$$\dot{M} = -\frac{R^4 P\pi}{8\mu R_{spec} T}\frac{dP}{dx}(1 + 8Kn) + \frac{3}{4}\frac{\pi\mu R^2}{T}\frac{dT}{dx}, \tag{50}$$

with R the radius and R_{spec} the specific gas constant.

Now since the pipe is closed and there is no inflow or outflow, at the start the thermal creep causes the fluid to flow from the cold to the hot side on the walls ($r = R$), this creates a pressure difference, which then creates a back flow in the middle (around $r = 0$). Under this condition we have zero mass flow rate, so we can calculate the pressure difference from equation (50):

$$P_2 - P_1 = \left(\frac{6\mu^2 R_{spec}}{R^2 P}\right)\frac{T_2 - T_1}{1 + 8Kn}. \quad (51)$$

Moreover, the pressure difference at equilibrium can also be combined with equation (48) to find an analytical solution for the velocity profile.

The results from the simulation compared to equaton (51) are shown in Figure 9.

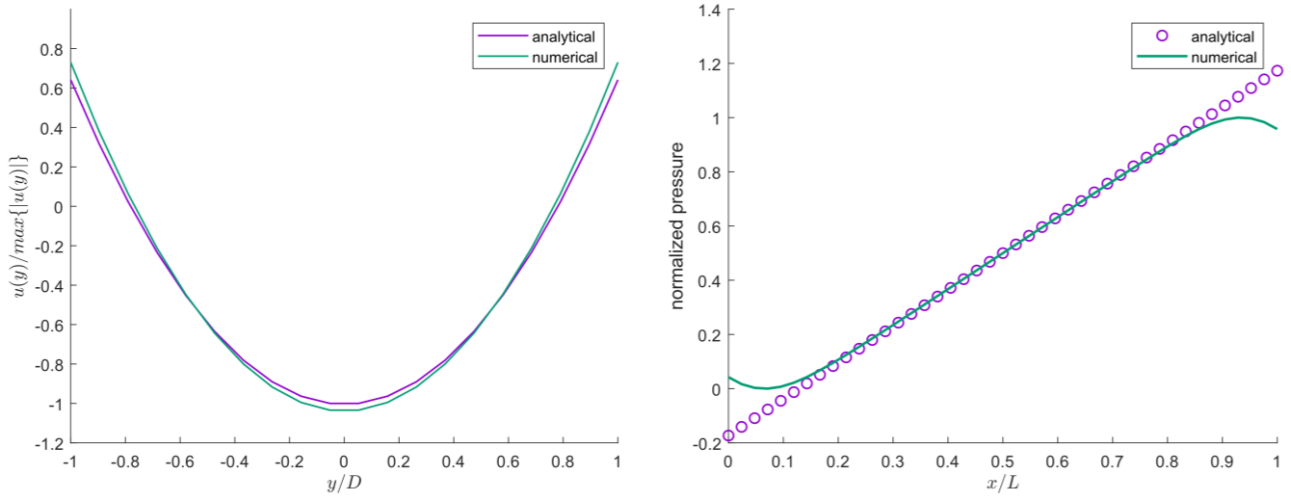

(a) (b)

Figure 9: Simulation results for *Kn*=0.053 with the geometry shown in Figure 2Error! Reference source not found.: (a) Normalized velocity profile along y-axis, (b) normalized pressure values along x-axis

As can be seen in Figure 9a, the velocity profile between analytical and numerical results agree very well. The pressure values in Figure 9b also agree with the prediction from equation (51) away from the left and right boundaries, but we notice a deviation near the walls. This can be attributed to the fact that the fluid needs to reverse its direction (cold to hot on the outer boundary, hot to cold in the middle), which creates this higher / lower pressure regions where the fluid coming from the upper wall meets the fluid coming from the lower wall. This effect is not considered in equation (51), as the latter doesn't take into account the vortex created by the fluid near walls. This can be better seen in Figure 10.

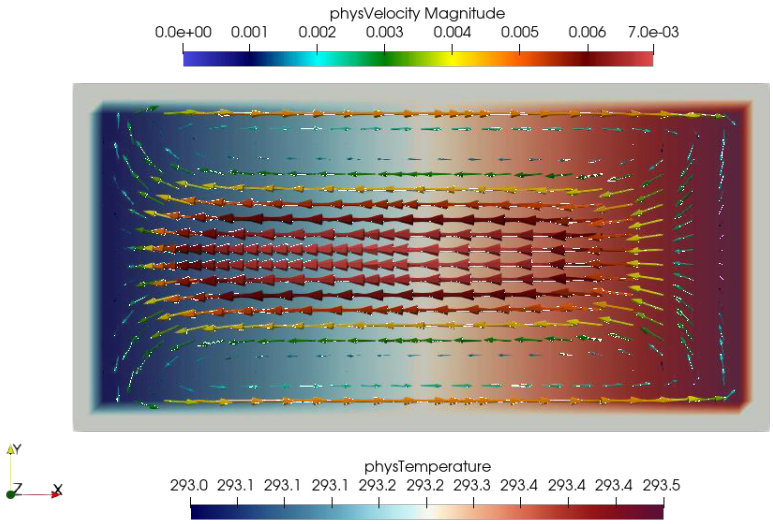

Figure 10: Fluid motion. The background shows the temperature heatmap for a Δ*T*=0.5, and the arrows show the direction of the fluid velocity for *Kn*=0.052

These results can be improved by adding a container on the left and right of the pipe with constant temperatures as shown in Figure 11, this helps regulate the pressure at the left and right walls.

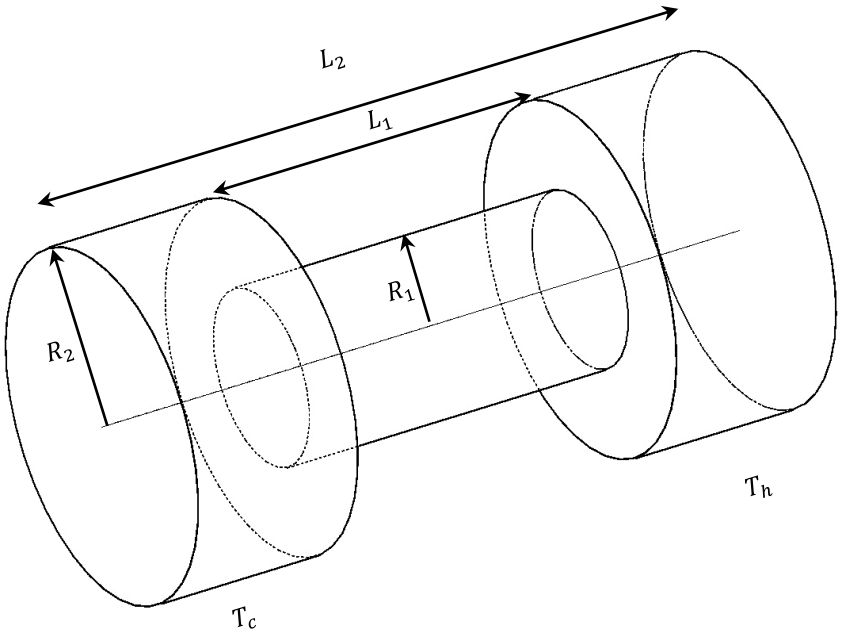

Figure 11: Simulation geometry with buffers on the left and right with $R^2 = 10^{-6}$ m, $R_1 = 5.10^{-7}$ m, $L_1 = 2.10^{-6}$ m and $L_2 = 4.10^{-6}$ m. The temperature at the right buffer is kept constant at $T_c = 293K$ and at the left one at $T_h = 293.5K$. The Knudsen number is $Kn = 0.052$ and the smaller pipe with radius R_1 has a linear change in temperature on its walls from T_c to T_h.

The simulation with the new geometry gives results that agree better with the analytical solution from equation (51).

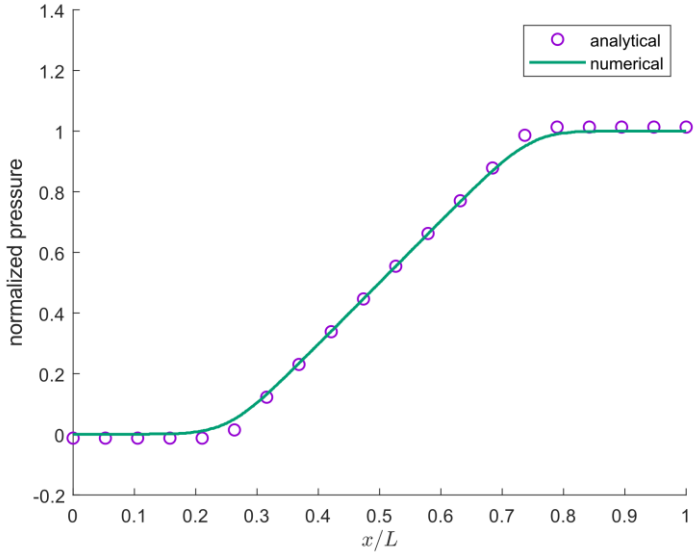

Figure 12: Normalized pressure values along x-axis for a simulation with the geometry shown in Figure 11 for $Kn = 0.053$.

4. Discussion

To simulate flows at higher Knudsen numbers, wall slip effects must be considered. In the isothermal case, it was shown that the general slip works well with the LBM and especially if paired with the Bouzidi implementation for the velocity, as this increases the order of convergence that would usually not exceed the first order due to the special discretization in uniform grid [4]. The interpolation used for the velocity at walls is usually used in the context of no-slip boundaries for the LBM, but we have shown it can also be used for slip boundaries. It was proven that the experimental order of convergence exceeds the first order using these boundary conditions which can have a big influence in a simulation where the boundaries are more complex and have

a significant effect on the flow. This can be further improved if more advanced slip models are used such as second order in Kn instead of only first order, or other combination of first and second order terms in Kn with different constants to further refine the accuracy under certain conditions as a lot of works tried to do. In fact, the idea behind this work is to combine slip models with the Bouzidi implementation for wall velocity and prove this works in a more general 3-dimensional case, which was not studied in other works.

Additionally, in the thermal case, the same can be done for the thermal creep velocity, which can also be paired with the Bouzidi interpolation in the same way the slip was combined with it [4]. An analytical solution was calculated for the equilibrium state in a 3-dimensional Knudsen pump, contrary to what is available in which only works in a simplified 2-dimensional setup and the simulation results show good agreement with it [1]. Although this work looks theoretical and no experimental or practical use was shown here, it is in fact a preparation for comparing measurement results and simulations. In fact, as was explained in the introduction, the velocity slip and thermal creep effects are very important at high Knudsen numbers, which is exactly the case for MEMS simulations. And when such a sensor is subject to an outside temperature gradient, it was observed that a new error is measured. This error is mainly caused by the temperature gradient, which as we have shown in this work can cause fluid movement by itself. Thus, the first step to simulating complex structures such as sensors, was done in this work, which is to study and characterize the boundary conditions, and the next step would be to apply these boundary conditions on a complex geometry and compare the results to measurements we are doing in the meantime [9,10,13].

Author Contributions

Conceptualization, A.S., M.J.K. and F.B.; methodology, A.S., M.J.K and F.B.; software, A.S.; validation, A.S.; formal analysis, A.S.; investigation, A.S.; resources, A.S. and C.N.; data curation, A.S.; writing—original draft preparation, A.S.; writing—review and editing, A.S., F.B., M.J.K and C.N.; visualization, A.S.; supervision, M.J.K. and C.N.; project administration, A.S. and M.J.K; funding acquisition, A.S. and C.N. All authors have read and agreed to the published version of the manuscript.

Acknowledgments

In this section, you can acknowledge any support given which is not covered by the author contribution or funding sections. This may include administrative and technical support, or donations in kind (e.g., materials used for experiments).

References

1. Karniadakis, G., Beskok, A., & Aluru, N. (2005). Microflows and nanoflows: fundamentals and simulation. New York, NY: Springer New York.
2. Succi, S. (2002). Mesoscopic modeling of slip motion at fluid-solid interfaces with heterogeneous catalysis. Physical review letters, 89(6), 064502.
3. Guo, Z., Zhao, T. S., & Shi, Y. (2006). Physical symmetry, spatial accuracy, and relaxation time of the lattice Boltzmann equation for microgas flows. Journal of Applied physics, 99(7).
4. Bouzidi, M. H., Firdaouss, M., & Lallemand, P. (2001). Momentum transfer of a Boltzmann-lattice fluid with boundaries. Physics of fluids, 13(11), 3452-3459.
5. Krause, M. J., Kummerländer, A., Avis, S. J., Kusumaatmaja, H., Dapelo, D., Klemens, F., ... & Simonis, S. (2021). OpenLB—Open source lattice Boltzmann code. Computers & Mathematics with Applications, 81, 258-288.
6. Krüger, T., Kusumaatmaja, H., Kuzmin, A., Shardt, O., Silva, G., & Viggen, E. M. (2017). The lattice Boltzmann method (Vol. 10, No. 978-3, pp. 4-15). Cham: Springer International Publishing.
7. Li, Q., He, Y. L., Tang, G. H., & Tao, W. Q. (2011). Lattice Boltzmann modeling of microchannel flows in the transition flow regime. Microfluidics and nanofluidics, 10(3), 607-618.
8. Kunze, S., Groll, R., Besser, B., & Thöming, J. (2022). Molecular diameters of rarefied gases. Scientific Reports, 12(1), 2057.
9. Gaedtke, M., Wachter, S., Kunkel, S., Sonnick, S., Rädle, M., Nirschl, H., & Krause, M. J. (2020). Nu-merical study on the application of vacuum insulation panels and a latent heat storage for refrigerated vehicles with a large Eddy lattice Boltzmann method. Heat and Mass Transfer, 56(4), 1189-1201.
10. Gaedtke, M., Wachter, S., Raedle, M., Nirschl, H., & Krause, M. J. (2018). Application of a lattice Boltzmann method combined with a Smagorinsky turbulence model to spatially resolved heat flux inside a refrigerated vehicle. Computers & Mathematics with Applications, 76(10), 2315-2329.
11. Nagel, C., Ante, F., Putnik, M., Classen, J., & Mehner, J. (2016). Characterization of temperature gradients on MEMS acceleration sensors. Procedia Engineering, 168, 888-891.
12. Selmi, A., Bhapkar, S., Nagel, C., Kummerländer, A., & Krause, M. J. (2023, April). Simulation of temperature driven microflows using a Lattice Boltzmann method in slip and moderate transition regimes. In 2023 24th International Conference on Thermal, Mechanical and Multi-Physics Simulation and Ex-periments in Microelectronics and Microsystems (EuroSimE) (pp. 1-6). IEEE.
13. Sbragaglia, M., & Succi, S. (2005). Analytical calculation of slip flow in lattice Boltzmann models with kinetic boundary conditions. Physics of Fluids, 17(9).